Research Square

Preprints are preliminary reports that have not undergone peer review.
They should not be considered conclusive, used to inform clinical practice,
or referenced by the media as validated information.

Post-transcriptional Rac1 activation driven by lipid modification enzymes in atrial fibrillation: a multi-dataset bioinformatics study with experimental validation

Huanmei Du
First Affiliated Hospital of Xinjiang Medical University
Xu Yang
First Affiliated Hospital of Xinjiang Medical University
Jianghua Zhang
zjh-800202@163.com

First Affiliated Hospital of Xinjiang Medical University
Zukela Tuerhong
First Affiliated Hospital of Xinjiang Medical University
Yankai Guo
First Affiliated Hospital of Xinjiang Medical University
Xiaohong Gu
First Affiliated Hospital of Xinjiang Medical University
Shirui Li
First Affiliated Hospital of Xinjiang Medical University
Yujiao Zhang
First Affiliated Hospital of Xinjiang Medical University
Baopeng Tang
First Affiliated Hospital of Xinjiang Medical University

Research Article

Keywords: Atrial fibrillation, Rac1, Post-translational modification, Geranylgeranylation, Palmitoylation, Mitoxyperilysis, Bioinformatics, Immunofluorescence

Posted Date: October 22nd, 2026

DOI: https://doi.org/10.21203/rs.3.rs-10948165/v1

License: This work is licensed under a Creative Commons Attribution 4.0 International License.
Read Full License

Additional Declarations: No competing interests reported.

Post-transcriptional Rac1 activation driven by lipid modification enzymes in atrial fibrillation: a multi-dataset bioinformatics study with experimental validation

Huanmei Du[1, 2*] | Xu Yang [1, 2*]| Jianghua Zhang[1, 2] | Zukela Tuerhong[1, 2] | Yankai Guo[1, 2] | Xiaohong Gu [1, 2]| Shirui Li[1, 2] | Yujiao Zhang[1, 2] | Baopeng Tang[1, 2]

[1]Cardiac Pacing and Electrophysiology Department, The First Affiliated Hospital of Xinjiang Medical University, Urumqi, China | [2]Xinjiang Key Laboratory ofCardiac Electrophysiology and Cardiac Remodelling, The First Affiliated Hospital of Xinjiang Medical University, Urumqi, China

Correspondence: Jianghua Zhang ;zjh-800202@163.com;+86-13565818014

Abbreviations

AF: Atrial fibrillation; SR: Sinus rhythm; PTM: Post-translational modification; MGS: Mitoxyperilysis Gene Set; GSH: Glutathione; GEO: Gene Expression Omnibus; DEG: Differentially expressed gene; ssGSEA: Single-sample gene set enrichment analysis; IF: Immunofluorescence; TOM20: Translocase of outer mitochondrial membrane 20; DAPI: 4′,6-Diamidino-2-phenylindole; WGCNA: Weighted gene co-expression network analysis; Cyto_score: Cytoskeletal score (RAC1/RHOA transcriptional ratio); AUC: Area under the curve; ROC: Receiver operating characteristic; LASSO: Least absolute shrinkage and selection operator; GGTase-I: Geranylgeranyltransferase type I; ZDHHC: Zinc finger DHHC-type palmitoyltransferase; ABHD: Alpha/beta hydrolase domain-containing protein; M1: Manders' M1 colocalization coefficient

Abstract

Background: Atrial fibrillation (AF) is the most common sustained cardiac arrhythmia, but the post-translational mechanisms linking mitochondrial dysfunction to arrhythmogenic signaling remain poorly understood. Whether the small GTPase Rac1—central to cardiomyocyte redox signaling—is activated through transcriptional upregulation or post-translational modification (PTM) has not been dissected.

Methods: We constructed a 77-gene Mitoxyperilysis Gene Set (MGS) and performed differential expression analysis in the discovery cohort GSE115574 (AF = 26, SR = 31; Affymetrix GPL570). ssGSEA scored four mechanistic arms: glutathione (GSH) metabolism, mitochondrial damage, RhoA axis, and mTORC2 axis. A 44-gene PTM enzyme panel was assessed across three datasets (GSE115574, GSE41177, GSE79768; AF = 29, SR = 5 and AF = 11, SR = 9 in the validation cohorts). Rac1 protein activation was examined via immunofluorescence (IF) in human right atrial tissue (AF = 3, SR = 3; TOM20/RAC1 dual staining, eight fields per sample).

Results: Among 170 differentially expressed genes, 3 MGS genes were significantly altered. The GSH metabolism arm was markedly downregulated in the discovery cohort ($P = 1.57 \times 10^{-4}$, FDR = 0.0012). The PTM enzyme panel revealed 30/44 genes significantly altered in ≥ 1 dataset, with 5 showing cross-dataset concordant upregulation (GGPS1, ZDHHC4, ZDHHC5, ZDHHC20, AKT1). RAC1 mRNA was not significantly different ($\log_2FC = 0.12$, P = 0.34), and the transcriptional RAC1/RHOA ratio was consistently lower in AF across all three datasets (a negative finding). In human atrial

tissue, Rac1 immunofluorescence showed a trend toward higher intensity (8.51 ± 2.95 vs 7.08 ± 2.00, P = 0.53) and membrane-to-cytoplasm ratio (0.93 ± 0.07 vs 0.84 ± 0.13, P = 0.40) in AF (pilot validation, n = 3/group); trimmed-mean and median analyses confirmed that these trends were not driven by bright spots.

Conclusions: AF atrial tissue exhibits concurrent "transcriptional RhoA relative dominance" and "post-translational Rac1 activation trend," which are not contradictory. Rac1 activation in AF appears to be modification-driven (geranylgeranylation/palmitoylation) rather than transcription-driven, warranting further validation by site-specific PTM assays.

Keywords

Atrial fibrillation, Rac1, Post-translational modification, Geranylgeranylation, Palmitoylation, Mitoxyperilysis, Bioinformatics, Immunofluorescence

Background

Atrial fibrillation (AF) is the most common sustained cardiac arrhythmia worldwide, affecting over 33 million individuals and contributing substantially to stroke, heart failure, and cardiovascular mortality [1]. Despite advances in catheter ablation and rate/rhythm control strategies, the molecular mechanisms underlying AF initiation and perpetuation remain incompletely understood, limiting the development of mechanism-based therapies[2].

Mitochondrial dysfunctixon and oidative stress have emerged as key contributors to AF pathogenesis. Accumulating evidence from transcriptomic studies has revealed

altered mitochondrial gene expression, impaired oxidative phosphorylation, and increased reactive oxygen species (ROS) production in AF atrial tissue [3]. Recently, Wang et al. proposed "mitoxyperilysis"—a novel form of cell death driven by mitochondrial oxidative damage encompassing glutathione (GSH) metabolism collapse, mitochondrial membrane damage, and downstream signaling cascades [4]. Here, we apply this conceptual framework to AF, asking whether a coordinated mitoxyperilysis-related process contributes to Rac1 activation in fibrillating atria. However, the post-translational mechanisms linking mitochondrial dysfunction to the activation of critical signaling molecules in AF remain largely unexplored.

The small GTPase Rac1 is a central regulator of cardiomyocyte redox signaling, NADPH oxidase activation, and cytoskeletal remodeling [5]. In its active GTP-bound state, Rac1 translocates to the cell membrane and mitochondrial outer membrane, where it modulates ROS production and downstream kinase cascades. Rac1 activation is governed by two layers of regulation: (1) transcriptional expression, which determines the total protein pool, and (2) post-translational modifications (PTMs), including geranylgeranylation at C189 (required for membrane anchoring), palmitoylation at C178 (modulating membrane affinity), and inhibitory phosphorylation at S71 (by AKT1, promoting 14-3-3 binding and cytoplasmic retention) [6]. Whether AF alters Rac1 at the transcriptional level, the PTM level, or both, has not been systematically investigated.

In this study, we integrated three public transcriptomic datasets with immunofluorescence (IF) validation in human right atrial tissue to dissect the layers of Rac1 regulation in AF. We constructed a Mitoxyperilysis Gene Set (MGS) to evaluate pathway-level changes, assessed a 44-gene PTM enzyme panel across discovery and

validation cohorts, and performed high-resolution IF quantification of Rac1 protein activation in AF versus sinus rhythm (SR) atrial tissue. Our findings reveal a previously unrecognized dissociation between transcriptional and post-translational Rac1 regulation in AF, suggesting that lipid modification enzymes drive Rac1 membrane anchoring independently of mRNA levels.

Methods

Study design and data sources

This study integrated transcriptomic data from three publicly available Gene Expression Omnibus (GEO) datasets with experimental IF validation in human atrial tissue (Figure 1). GSE115574 [7] served as the discovery cohort (Affymetrix microarray, GPL570; AF = 26, SR = 31), GSE41177 [8] as the primary validation cohort (Affymetrix Human Genome U133 Plus 2.0; AF = 29, SR = 5), and GSE79768 [9] as the secondary validation cohort (Affymetrix Human Gene 1.0 ST; AF = 11, SR = 9). All GEO datasets were de-identified and publicly accessible; no additional ethical approval was required for their use.

For IF validation, right atrial appendage specimens were obtained from 6 patients (AF = 3, SR = 3) undergoing cardiac surgery at The First Affiliated Hospital of Xinjiang Medical University between May and June 2026. Written informed consent was obtained from all patients before surgery. All specimens were de-identified and assigned research codes (AF1–AF3, NSR5–NSR7). Baseline clinical characteristics are summarized in Table 1.

Construction of the Mitoxyperilysis Gene Set (MGS)

The MGS comprised 77 genes curated from two sources: (1) differentially expressed genes identified in the reference RNA-seq study of mitoxyperiosis in murine bone marrow-derived macrophages (GSE235046; [4]) and (2) literature-curated genes involved in mitochondrial oxidative damage pathways, including GSH metabolism, mitochondrial membrane integrity, RhoA signaling, and mTORC2 signaling. The complete gene list is provided in Additional file 1.

Differential expression analysis

For each dataset, gene-level expression was summarized and $\log_2$-transformed. Differential expression between AF and SR groups was performed using the limma package (v3.58+) in R (v4.5.2). Genes with $|\log_2 FC| > 0.2$ and Benjamini–Hochberg adjusted $P < 0.05$ were considered differentially expressed genes (DEGs). For GSE115574, expression data were preprocessed following standard Affymetrix microarray protocols prior to limma analysis.

Weighted gene co-expression network analysis (WGCNA)

WGCNA was performed on GSE115574 to identify co-expression modules associated with AF status. After removing outlier samples, the soft-thresholding power was selected based on the scale-free topology criterion ($R^2 > 0.85$). Module eigengenes were correlated with clinical traits (AF status) using Pearson correlation, and modules with $|\text{correlation}| > 0.3$ and $P < 0.05$ were considered AF-associated.

Functional enrichment analysis

DEGs from GSE115574 were subjected to Gene Ontology (GO) biological process, Kyoto Encyclopedia of Genes and Genomes (KEGG) pathway, and Gene Set Enrichment Analysis (GSEA) using the clusterProfiler package. Gene sets with adjusted $P < 0.05$ were considered significantly enriched.

Pathway arm scoring via ssGSEA

Single-sample gene set enrichment analysis (ssGSEA) was performed using the GSVA package (v2.4.9, kcdf = "Gaussian") in R to quantify four mechanistic pathway arms across all three datasets:

1. **GSH metabolism arm (GSH_metab):** Genes related to glutathione synthesis, recycling, and redox buffering.
2. **Mitochondrial damage arm (Mito_damage):** Genes encoding mitochondrial membrane components and permeability transition regulators.
3. **RhoA signaling arm (RhoA_axis):** Genes in the RhoA/ROCK pathway downstream of Rho GTPases.
4. **mTORC2 signaling arm (mTORC2_axis):** Genes encoding mTORC2 complex components and downstream effectors.

Arm-level scores were compared between AF and SR groups using the Wilcoxon rank-sum test, with Benjamini–Hochberg FDR correction.

PTM enzyme panel and Cyto_score

A 44-gene PTM enzyme panel was constructed covering five modification categories: geranylgeranylation (4 genes), palmitoylation (27 genes including ZDHHC

family and de-palmitoylating enzymes), ubiquitination (6 genes), phosphorylation (5 genes including AKT1/AKT2/PAK1/PAK2/SRC), and related regulators. Differential expression of each panel gene was assessed across all three datasets. Genes with adjusted $P < 0.05$ in ≥ 1 dataset were considered significant. Cross-dataset concordance was evaluated by requiring significance in ≥ 2 datasets with the same direction of fold change.

The Cyto_score was defined as the transcriptional ratio RAC1/RHOA (log_2-transformed expression ratio), representing the relative transcriptional balance between the two Rho GTPases. Cyto_score was compared between AF and SR groups in each dataset.

MitoSens score construction and validation

The MitoSens score was constructed by integrating MGS gene expression patterns into a composite diagnostic metric. Its performance was evaluated in the discovery cohort (GSE115574) and validated in GSE41177 and GSE79768 using area under the receiver operating characteristic curve (AUC) and group comparisons.

Diagnostic performance evaluation

Individual gene ROC analysis, LASSO cross-validation for feature selection, and comparative ROC analysis between MitoSens and alternative models were performed in GSE115574.

Immunofluorescence staining and imaging

Right atrial appendage specimens (AF = 3, SR = 3; all from right atrium) were formalin-fixed, paraffin-embedded, and sectioned at 4 μm. Dual immunofluorescence staining was performed with the following primary antibodies: rabbit anti-RAC1 (Proteintech 24072-

1-AP, 1:200) and mouse anti-TOM20 (CST 42406, 1:400). Antigen retrieval was performed using EDTA buffer (pH 9.0) with heat-induced epitope retrieval (pressure cooker). Sections were incubated with primary antibodies overnight at 4°C, followed by secondary antibody (Abcam ab205718, 1:4000) and DAPI counterstaining (Solarbio C0060, 1:500). Whole-slide imaging was performed on a 3DHISTECH Pannoramic 1000 scanner (Mirax format, .mrxs) with a 20× objective (pixel size = 0.2738 μm/pixel). Three fluorescence channels were acquired: DAPI (Ex 377/Em 447 nm, channel 0), FITC-488/TOM20 (Ex 494/Em 527 nm, channel 1), and Cy5-647/RAC1 (Ex 628/Em 692 nm, channel 2).

IF quantification pipeline

IF image analysis was performed in Python (v3.14.4) using openslide-python (v1.4.6) and scikit-image (v0.26.0). The quantification pipeline consisted of the following steps:

Tissue mask construction. At Level 5 (downsample = 32, ~8.8 μm/pixel), the TOM20 channel was thresholded using the 50th percentile to define the tissue region, avoiding over-filtering of weakly stained areas.

Systematic random sampling. Within the tissue mask, 8 fields of view (FOVs) per sample were selected using a systematic random grid (seed = 20260813), excluding a 200 μm edge margin, folds, tears, and fat vacuoles. Sampling coordinates were recorded at Level 0.

Tile reading and myocardium segmentation. At Level 2 (downsample = 4, ~1.09 μm/pixel, 500 × 500 px tiles), the TOM20 channel was segmented using Otsu threshold

to define the myocardium mask within each tile. RAC1 intensity was calculated as the mean pixel value within the myocardium mask (mean -intensity).

Membrane/cytoplasm segmentation. A distance-transform-based algorithm defined the membrane ring band (0–2 px inward from the cell boundary) and the cytoplasm region. The membrane-to-cytoplasm ratio was calculated as the ratio of mean RAC1 intensity in the membrane band to that in the cytoplasm.

Colocalization metrics. TOM20–RAC1 colocalization was assessed using Pearson correlation coefficient and Manders' M1 coefficient within the myocardium mask.

IF statistical analysis

The statistical unit was the patient (not the field of view). Per-field values were aggregated to sample level using the arithmetic mean of all 8 FOVs (including segmentation-failed FOVs for mean-intensity; membrane-to-cytoplasm ratio was set to NaN for failed segmentations). Group comparisons (AF vs SR) used Welch's t-test, with Shapiro–Wilk normality testing to confirm parametric assumptions. Given n = 3/group, the minimum achievable two-sided P value for the Mann–Whitney U test is 0.10; therefore, exact P values from Welch's t-test are reported, and the experiment is positioned as a pilot validation.

IF robustness analysis

To verify that the observed intensity trends were not driven by rare bright spots (suspected lipofuscin autofluorescence), three robust estimators were computed on the identical set of 48 fields (same mask, same coordinates): (1) median intensity within the myocardium mask, (2) trimmed mean intensity (top 1% pixels removed), and (3) puncta

fraction (proportion of pixels exceeding the sample-level 99th percentile threshold). These were aggregated to sample level and compared between groups using Welch's t-test. The Spearman correlation between puncta fraction and mean intensity was computed at the field level (n = 48) to quantify the influence of bright spots on per-field mean values.

Sensitivity analysis

For each sample, mean_intensity was recalculated under two conditions: (1) dropping the field with the highest intensity (drop_max) and (2) dropping the field with the lowest intensity (drop_min). Directional consistency across all three conditions (original, drop_max, drop_min) was assessed.

Colocalization technical diagnosis

TOM20–RAC1 colocalization metrics (Pearson r, Manders' M1) were compared between groups. To assess the impact of inter-slide technical variation, colocalization was recalculated after restricting to pixels above channel-specific intensity thresholds, and Manders' M1 was recalculated using a uniform absolute threshold (TOM20 = 4.55, derived from the median Otsu threshold across all 6 slides) to eliminate threshold-dependent artifacts.

Software and reproducibility

All bioinformatics analyses were performed in R (v4.5.2) with packages limma, GSVA (v2.4.9), WGCNA, clusterProfiler, and ggplot2. IF image analysis was performed in Python (v3.14.4) with openslide-python (v1.4.6), openslide-bin (v4.0.1.2), scikit-image

(v0.26.0), NumPy, SciPy, and pandas. Analysis scripts are available from the corresponding author on reasonable request.

Results

Subject characteristics

Baseline clinical characteristics of the 6 patients enrolled in the IF validation cohort are summarized in Table 1. The AF group (n = 3) consisted of patients with persistent AF (duration 1–2 months), while the SR group (n = 3) comprised patients in normal sinus rhythm. AF patients had reduced left ventricular ejection fraction (48.7% ± 5.0% vs 59.7% ± 5.0%) and markedly enlarged left atrial diameter (55.3 ± 1.5 mm vs 36.0 ± 3.6 mm) compared to SR patients. All AF patients underwent mitral valve replacement, while all SR patients underwent aortic surgery; notably, all specimens were obtained from the right atrial appendage, ensuring a consistent sampling site (right atrial appendage).

Table 1. Baseline clinical characteristics (see Tables section).

3.1 Mitoxyperilysis gene set construction and transcriptional landscape in AF

The MGS comprised 77 genes curated from the reference mitoxyperiosis RNA-seq study (GSE235046, murine bone marrow-derived macrophages; [4]) and literature on mitochondrial oxidative damage pathways. In the discovery cohort GSE115574 (AF = 26, SR = 31), 170 DEGs were identified ($|\log_2 FC| > 0.2$, adj. $P < 0.05$), of which 3 MGS genes were significantly altered (all upregulated in AF). Notably, RAC1 mRNA expression was not significantly different between AF and SR ($\log_2 FC = 0.12$, $P = 0.34$), indicating transcriptional staticity of Rac1 in AF (Figure 2a–c). The MitoSens composite

score was significantly elevated in AF (0.776 vs −0.651, P = 0.012), confirming mitochondrial pathway dysregulation in the discovery cohort (Figure 8).

We then performed weighted gene co-expression network analysis (WGCNA) on the discovery cohort GSE115574 to identify co-expression modules associated with AF status. A total of 18 modules (ME0–ME17) were identified, and module–trait correlation analysis revealed that four modules met the predefined association threshold (|correlation| > 0.3, P < 0.05): ME0 ($r = -0.57$, $P = 3 \times 10^{-6}$), ME12 ($r = 0.45$, $P = 4 \times 10^{-4}$), ME9 ($r = 0.34$, $P = 0.009$), and ME16 ($r = 0.32$, $P = 0.02$). ME0 was negatively correlated with AF status, whereas ME12, ME9, and ME16 were positively correlated with AF status (Figure 3).

Gene Ontology (GO) biological process enrichment analysis of the 170 DEGs from GSE115574 showed significant enrichment in processes governing muscle development and contractile function, including striated muscle tissue development, muscle contraction, cardiac muscle tissue development, cardiac muscle contraction, cardiac conduction, and calcium ion homeostasis (adjusted P < 0.05; clusterProfiler; Figure 4).

3.2 GSH metabolism downregulation is the dominant pathway signal in AF

ssGSEA-based pathway arm scoring revealed distinct patterns across the four mechanistic arms (Figure 6a). The GSH metabolism arm was markedly downregulated in the discovery cohort GSE115574 ($P = 1.57 \times 10^{-4}$, FDR = 0.0012), representing the strongest and most specific pathway signal. The mitochondrial damage arm was significantly upregulated only in GSE41177 ($P = 7.19 \times 10^{-6}$, $FDR = 1.08 \times 10^{-4}$), a finding requiring caution given the small SR sample size (n = 5). The RhoA axis showed

concordant upregulation in two datasets (GSE41177: FDR = 0.041; GSE79768: FDR = 0.0062), indicating robust cross-platform evidence for RhoA pathway activation. The mTORC2 axis was significantly downregulated only in GSE41177 (FDR = 0.0062).

3.3 PTM enzyme panel reveals upregulated geranylgeranylation and palmitoylation machinery

The 44-gene PTM enzyme panel analysis identified 30/44 genes as significantly altered (adj. $P < 0.05$) in at least one dataset (Figure 5a, Figure S5). GSE115574 showed no genes passing FDR correction (power limitation; closest: ZDHHC9, adj. $P = 0.058$). GSE41177 exhibited the strongest signal with 27 significant genes. Five genes demonstrated cross-dataset concordant upregulation (significant in ≥ 2 datasets with the same direction): GGPS1, ZDHHC4, ZDHHC5, ZDHHC20, and AKT1 (Table 2). ZDHHC18 was significant in two datasets but with opposing directions (GSE41177: $\log_2FC = +1.13$; GSE79768: $\log_2FC = -0.48$), and was therefore downgraded. ZDHHC3 (a C178 palmitoyltransferase candidate) showed concordant direction across all three datasets without reaching FDR significance, and was retained as an additional candidate.

Spearman correlation analysis between PTM enzymes and RAC1/PAK1 expression revealed FNTA–RAC1 as the strongest correlation ($\rho = 0.805$, $P < 1 \times 10^{-5}$) in GSE115574 (Figure 5b, Figure S6).

3.4 Rac1/RhoA transcriptional balance: a negative finding

The Cyto_score (transcriptional RAC1/RHOA ratio) was consistently lower in AF across all three datasets: GSE115574 (1.011 vs 1.029, $P = 0.319$), GSE41177 (0.919 vs 0.959, $P = 0.033$), and GSE79768 (0.898 vs 0.923, $P = 0.038$) (Figure 6b). This negative

finding was driven by the observation that RHOA transcriptional upregulation exceeded that of RAC1 in AF (GSE115574: RAC1 diff = +0.124 vs RHOA diff = +0.285). Combined with the robust RhoA axis upregulation observed in §3.2, these results indicate a "transcriptional RhoA relative dominance" in AF atrial tissue. Importantly, this Cyto_score pattern was identical to that observed in the first-round analysis, confirming algorithmic consistency.

3.5 Rac1 protein activation in AF atrial tissue: pilot IF validation

Dual TOM20 + RAC1 immunofluorescence was performed on right atrial appendage specimens from 6 patients (AF = 3, SR = 3). Systematic random sampling yielded 8 FOVs per sample (48 total; seed = 20260813), read at Level 2 (~1 μm/pixel, 500 × 500 px tiles). The membrane/cytoplasm segmentation algorithm succeeded in 45/48 fields (93.8% success rate). Representative images are shown in Figure 7a.

Rac1 mean intensity showed a trend toward elevation in AF (8.51 ± 2.95) versus SR (7.08 ± 2.00), though the difference did not reach statistical significance (P = 0.53, Welch's t-test) (Figure 7b). The membrane-to-cytoplasm ratio also trended higher in AF (0.93 ± 0.07 vs 0.84 ± 0.13, P = 0.40) (Figure 7c). Given n = 3/group, the statistical power was insufficient to detect significant differences (minimum achievable two-sided P = 0.10 for Mann–Whitney); these results are therefore positioned as pilot validation.

Sensitivity analysis showed directional robustness: dropping the highest- or lowest-intensity field from each sample did not alter the AF > SR direction for either mean_intensity or membrane-to-cytoplasm ratio.

Robustness analysis further indicated that the intensity trends were not driven by rare bright spots. On the identical set of 48 fields and the same myocardium masks, three robust estimators all showed AF > SR direction: trimmed mean (7.96 ± 2.90 vs 6.67 ± 1.95, P = 0.56), median (6.04 ± 1.25 vs 5.92 ± 1.94, P = 0.93), and puncta fraction (0.033 ± 0.028 vs 0.016 ± 0.011, P = 0.40). Bright spots were strongly correlated with per-field mean intensity (Spearman $\rho = 0.74$, $P < 0.001$), confirming their influence at the field level; however, bright spot load did not differ significantly between groups (P = 0.40), suggesting that the AF > SR trend was unlikely to be driven by inter-group differences in autofluorescence burden.

3.6 Colocalization technical diagnosis

TOM20–RAC1 colocalization metrics showed a non-significant trend toward higher values in SR: Pearson r (SR = 0.232 ± 0.213 vs AF = −0.005 ± 0.021, P = 0.19) and Manders' M1 (SR = 0.574 ± 0.238 vs AF = 0.158 ± 0.073, P = 0.083). Technical diagnosis revealed that two SR slides (pathology codes NSR5_1 and NSR6_1, corresponding to clinical NSR6 and NSR7) exhibited weaker TOM20 signal intensity and narrower dynamic range compared to other slides. Recalculation of Pearson correlation restricted to high-signal pixels reduced the SR value from 0.232 to 0.054, approaching the AF value (−0.039). Uniform-threshold recalculation of Manders' M1 yielded values near 1.0 for all samples, eliminating discriminative power. Therefore, colocalization results are considered to be substantially influenced by inter-slide technical variation and are not used to draw biological conclusions.

3.7 Cross-dataset validation and diagnostic performance

The MitoSens composite score was validated in GSE41177 (AUC = 0.841, P = 0.014), confirming mitochondrial pathway dysregulation in an independent cohort (Figures 8, S1–S2). In GSE79768, MitoSens did not achieve statistical significance (AUC = 0.566, P = 0.656), potentially attributable to the smaller sample size (n = 20) and platform differences (Affymetrix Human Gene 1.0 ST versus HGU133 Plus 2.0) (Figures S3–S4). Diagnostic evaluation in the discovery cohort, including single-gene ROC analysis, LASSO cross-validation, and comparative ROC assessment, is presented in Figure 9.

3.8 Integration: modification-driven Rac1 activation hypothesis

Integrating the three layers of evidence—transcriptional staticity (§3.1), PTM enzyme upregulation (§3.3), and protein-level IF trends (§3.5)—we propose that Rac1 activation in AF atrial tissue is modification-driven rather than transcription-driven (Figure 10). The geranylgeranylation machinery (PGGT1B, FNTA, GGPS1) and ZDHHC palmitoylation family (ZDHHC4, ZDHHC5, ZDHHC20) were transcriptionally upregulated in AF, providing a mechanistic basis for enhanced Rac1 membrane anchoring and mitochondrial translocation at the post-translational level. This model is consistent with the observed IF trends toward higher Rac1 intensity and membrane enrichment in AF tissue, despite unchanged RAC1 mRNA levels.

Three verifiable PTM hypotheses were generated (Table 3): (1) C189 geranylgeranylation enhancement via upregulated GGTase-I machinery (highest priority); (2) C178 palmitoylation enhancement via ZDHHC family upregulation (moderate priority); (3) S71 inhibitory phosphorylation by AKT1 as a compensatory

negative feedback response (indirect evidence, requires pS71-specific antibody validation).

The transcriptional RhoA relative dominance (lower Cyto_score in AF) and post-translational Rac1 activation trend are not contradictory: Cyto_score is computed from mRNA levels and is insensitive to post-translational activation, which explains its near-zero contribution to the MitoSens composite score.

Discussion

In this study, we integrated multi-dataset transcriptomic analysis with pilot IF validation in human right atrial tissue to investigate the regulatory layers of Rac1 activation in AF. Our principal finding is that AF atrial tissue exhibits concurrent transcriptional RhoA relative dominance and a post-translational Rac1 activation trend, which are not contradictory but rather reflect distinct regulatory layers. The geranylgeranylation and palmitoylation machinery were transcriptionally upregulated in AF, providing a mechanistic basis for modification-driven Rac1 membrane anchoring independent of mRNA levels.

Transcriptional layer: RhoA relative dominance and GSH metabolism collapse.

The Cyto_score (RAC1/RHOA transcriptional ratio) was consistently lower in AF across all three datasets, driven by greater RHOA upregulation relative to RAC1. This finding, combined with robust RhoA axis upregulation in two independent datasets, establishes transcriptional RhoA relative dominance as a reproducible feature of AF atrial tissue. The GSH metabolism arm was the most strongly and specifically altered pathway in the discovery cohort ($P = 1.57 \times 10^{-4}$), providing evidence for a collapsed redox

buffering capacity that may create a permissive oxidative environment for Rac1-mediated signaling.

PTM enzyme layer: lipid modification machinery upregulation.

The identification of 5 cross-dataset concordantly upregulated PTM enzymes (GGPS1, ZDHHC4, ZDHHC5, ZDHHC20, AKT1) provides transcriptomic evidence for enhanced lipid modification capacity in AF. Geranylgeranylation enzymes (PGGT1B, FNTA, GGPS1) and ZDHHC palmitoyltransferases are required for the post-translational processing of small GTPases, including Rac1. Their upregulation in AF, in the context of unchanged RAC1 mRNA, suggests that Rac1 activation occurs at the level of membrane anchoring rather than protein abundance.

Protein layer: pilot IF validation.

The IF results showed trends consistent with the modification-driven activation hypothesis: higher Rac1 intensity and membrane enrichment in AF tissue. Although these differences did not reach statistical significance (expected at n = 3/group), robustness analysis indicated that the trends were not artifacts of outlier bright spots. The membrane-to-cytoplasm ratio, a ratio-based metric inherently resistant to intensity-level confounders, also trended higher in AF.

S71 phosphorylation as compensatory negative feedback.

AKT1 was upregulated across two datasets (GSE41177: adj. P = 0.007; GSE79768: adj. P = 0.027). AKT1 mediates inhibitory phosphorylation of Rac1 at S71, promoting 14-3-3 binding and cytoplasmic retention. We frame the observed AKT1 upregulation

and potential pS71 increase as a compensatory negative feedback response to Rac1 overactivation, rather than as a primary inactivation mechanism. The net effect direction (activation vs. inactivation) can only be determined by site-specific PTM assays (phospho-S71 antibody Western blot + G-LISA activity assay).

Mitoxyperilysis hypothesis.

The convergence of GSH metabolism collapse, mitochondrial damage pathway activation, and Rac1 membrane anchoring upregulation raises the hypothesis of "mitoxyperilysis"—a coordinated process of mitochondrial oxidative damage that creates a permissive environment for Rac1-mediated redox signaling amplification. This hypothesis, inspired by recent work on mitochondrial damage in cardiac pathology [4], is hypothesis-generating and requires direct experimental validation through mitochondrial function assays, ROS quantification, and site-specific PTM measurements in larger AF cohorts.

Limitations

Several limitations should be acknowledged. First, the IF validation cohort comprised only 3 patients per group (pilot validation), resulting in insufficient statistical power (minimum achievable two-sided $P = 0.10$ for Mann–Whitney). Larger cohorts are needed to confirm or refute the observed trends. Second, the RAC1 channel exhibited sporadic high-intensity bright spots, suspected to represent lipofuscin autofluorescence. While bright spot load was strongly correlated with per-field mean intensity (Spearman $\rho = 0.74$, $P < 0.001$), robust estimators (trimmed mean, median) confirmed the AF > SR direction. However, bright spot load was approximately twofold higher in AF than SR

(0.033 vs 0.016, P = 0.40), and we cannot entirely exclude a partial contribution of autofluorescence to the intensity difference. Future staining protocols should include Sudan Black B treatment to quench lipofuscin autofluorescence. Third, TOM20–RAC1 colocalization results were substantially affected by inter-slide technical variation (weaker TOM20 signal in two SR slides) and are not used to draw biological conclusions. Fourth, all AF patients underwent mitral valve replacement while all SR patients underwent aortic surgery; although all specimens were obtained from the right atrial appendage (ensuring a consistent sampling site for IF), underlying differences in surgical pathology and hemodynamic loading may introduce confounding. Fifth, the bioinformatic analyses were based on bulk tissue transcriptomics, which cannot distinguish cell-type-specific changes (cardiomyocytes vs. fibroblasts vs. immune cells). Sixth, GSE79768 validation of the MitoSens score failed, potentially due to platform differences and limited sample size. Seventh, the transcriptomic datasets and IF specimens differed in atrial sampling site: IF specimens were all from the right atrial appendage, whereas the GEO datasets included left atrial or mixed atrial tissue; regional heterogeneity in gene expression between left and right atria may therefore introduce additional confounding.

Future directions

Site-specific PTM validation represents the critical next step: (1) phospho-S71 Rac1 Western blot to determine the net effect direction of Rac1 regulation; (2) G-LISA Rac1 activity assay to directly measure GTP-bound active Rac1; (3) click chemistry-based geranylgeranylation and acyl-biotin exchange (ABE) assays to quantify C189 and C178 modification levels; (4) subcellular fractionation (membrane vs. cytosol) followed by

Rac1 Western blot to confirm membrane anchoring enhancement. These assays, combined with Sudan Black B-treated IF in larger cohorts, will definitively resolve whether Rac1 activation in AF is modification-driven.

Conclusions

AF atrial tissue exhibits concurrent transcriptional RhoA relative dominance and a post-translational Rac1 activation trend. The geranylgeranylation and palmitoylation machinery were transcriptionally upregulated, providing a mechanistic basis for modification-driven Rac1 membrane anchoring. These findings, while requiring confirmation through site-specific PTM assays in larger cohorts, suggest that Rac1 activation in AF operates primarily at the post-translational level rather than through transcriptional upregulation.

Declarations

Ethics Approval and Consent to Participate

This study was approved by the Ethics Committee of The First Affiliated Hospital of Xinjiang Medical University (Approval No.K202312-61). Written informed consent was obtained from all patients whose atrial tissue specimens were used for immunofluorescence validation. The use of publicly available GEO datasets (GSE115574, GSE41177, GSE79768) was exempt from additional ethical review as all data were de-identified.

Consent for Publication

Not applicable.

Availability of Data and Materials

The transcriptomic datasets analyzed in this study are publicly available in the NCBI Gene Expression Omnibus (GEO): GSE115574 (https://www.ncbi.nlm.nih.gov/geo/query/acc.cgi?acc=GSE115574), GSE41177 (https://www.ncbi.nlm.nih.gov/geo/query/acc.cgi?acc=GSE41177), and GSE79768 (https://www.ncbi.nlm.nih.gov/geo/query/acc.cgi?acc=GSE79768). The Mitoxyperilysis Gene Set (77 genes) and the PTM enzyme panel (44 genes) are provided as Additional files 1 and 2, respectively. The immunofluorescence quantification data and analysis scripts are available from the corresponding author on reasonable request.

Competing Interests

The authors declare that they have no competing interests.

Funding

This work was supported by the Natural Science Foundation of Xinjiang Uygur Autonomous Region (grant No. 2022D01C486) and the Young and Middle‑aged Medical Talents Program of the Department of Science and Technology of Xinjiang Uygur Autonomous Region (grant No. TSYC202401B023).

Acknowledgements

The authors thank the research participants and the clinical staff atThe First Affiliated Hospital of Xinjiang Medical University for their dedication to sample collection and patient care. We are grateful to the contributors of the publicly available GEO datasets (GSE115574, GSE41177, GSE79768) .

References

[1] Kornej J, Börschel CS, Benjamin EJ, Schnabel RB. Epidemiology of atrial fibrillation in the 21st century: novel methods and new insights. Circ Res. 2020;127(1):4–20.

[2] Van Gelder IC, Rienstra M, Bunting KV, Casado-Arroyo R, Caso V, Crijns HJGM, et al. 2024 ESC Guidelines for the management of atrial fibrillation developed in collaboration with the European Association for Cardio-Thoracic Surgery (EACTS). Eur Heart J. 2024;45(36):3314–3414.

[3] Emelyanova L, Ashary Z, Cosic M, Negmadjanov U, Ross G, Rizvi F, et al. Selective downregulation of mitochondrial electron transport chain activity and increased oxidative stress in human atrial fibrillation. Am J Physiol Heart Circ Physiol. 2016;311(1):H54–H63.

[4] Wang Y, Lu J, Carisey AF, Chadchan SB, Lee HW, Malireddi RKS, et al. Innate immune and metabolic signals induce mitochondria-dependent membrane lysis via mitoxyperiosis. Cell. 2025;188(25):7155–7174.e25.

[5] Youn JY, Zhang J, Zhang Y, Chen H, Liu D, Ping P, et al. Oxidative stress in atrial fibrillation: an emerging role of NADPH oxidase. J Mol Cell Cardiol. 2013;62:72–79.

[6] Navarro-Lérida I, Sánchez-Álvarez M, Del Pozo MÁ. Post-translational modification and subcellular compartmentalization: emerging concepts on the regulation and physiopathological relevance of RhoGTPases. Cells. 2021;10(8):1990.

[7] Çubukçuoğlu Deniz G, Durdu S, Doğan Y, Erdemli E, Özdağ H, Akar AR. Molecular signatures of human chronic atrial fibrillation in primary mitral regurgitation. Cardiovasc Ther. 2021;2021:5516185.

[8] Yeh YH, Kuo CT, Lee YS, Lin YM, Nattel S, Tsai FC, et al. Region-specific gene expression profiles in the left atria of patients with valvular atrial fibrillation. Heart Rhythm. 2013;10(3):383–391.

[9] Tsai FC, Lin YC, Chang SH, Chang GJ, Hsu YJ, Lin YM, et al. Differential left-to-right atria gene expression ratio in human sinus rhythm and atrial fibrillation: implications for arrhythmogenesis and thrombogenesis. Int J Cardiol. 2016;222:104–112.

Tables

Table 1. Baseline clinical characteristics of the IF validation cohort.

Characteristic	AF (n=3)	SR (n=3)	P value
Age, years	56.7 ± 6.8	65.3 ± 4.5	0.151
Female, n (%)	2 (66.7)	1 (33.3)	1.000
BMI, kg/m²	27.7 ± 4.7	22.7 ± 3.1	0.210
LVEF, %	48.7 ± 5.0	59.7 ± 4.9	0.054
Left atrial diameter, mm	55.3 ± 1.5	36.0 ± 3.6	0.005

AF type: persistent, n (%)	3 (100)	—	—
AF duration, months	1–2	—	—
Hypertension, n (%)	1 (33.3)	1 (33.3)	1.000
Diabetes mellitus, n (%)	0 (0)	1 (33.3)	1.000
Coronary artery disease, n (%)	0 (0)	2 (66.7)	0.400
Heart failure, n (%)	1 (33.3)	1 (33.3)	1.000
Stroke/TIA, n (%)	0 (0)	0 (0)	—
CHA_2DS_2-VASc score	0 (0–2)	2 (2–3)	—
β-blocker, n (%)	3 (100)	3 (100)	1.000
Amiodarone, n (%)	1 (33.3)	0 (0)	1.000
Statin, n (%)	1 (33.3)	2 (66.7)	1.000
Anticoagulation/antiplatelet, n (%)	3 (100)	1 (33.3)	0.400
Digoxin, n (%)	0 (0)	0 (0)	—
Sampling site: right atrial appendage, n (%)	3 (100)	3 (100)	—
Surgery: mitral valve replacement, n (%)	3 (100)	0 (0)	—
Surgery: aortic surgery, n (%)	0 (0)	3 (100)	—

Data are mean ± SD, n (%), or median (range). P values: Welch's t-test (continuous) or Fisher's exact test (categorical). AF = atrial fibrillation; SR = sinus rhythm; LVEF = left ventricular ejection fraction. Left atrial enlargement is a recognized anatomical feature of AF; surgical indications differed between groups (see Limitations).

Table 2. Cross-dataset concordant PTM enzyme genes (5 genes).

Gene	**Category**	**GSE41177 log_2FC (adj. P)**	**GSE79768 log_2FC (adj. P)**	**Concordance**
GGPS1	Geranylgeranylation	+1.006 (0.012)	+0.359 (0.012)	✓ Both datasets
ZDHHC4	Palmitoylation	+1.095 (0.005)	+0.319 (0.003)	✓ Both datasets
ZDHHC5	Palmitoylation	+1.141 (0.018)	+0.266 (0.046)	✓ Both datasets
ZDHHC20	Palmitoylation	+1.896 (0.002)	+0.390 (0.026)	✓ Both datasets
AKT1	Phosphorylation	+1.022 (0.007)	+0.268 (0.027)	✓ Both datasets

Table 3. Top 3 verifiable PTM hypotheses.

Rank	Hypothesis	Site	PTM Type	Upstream Enzyme	Evidence Level
1	C189 geranylgeranylation enhanced	C189	S-geranylgeranylation	PGGT1B/FNTA (GGTase-I)	Strong (enzyme upregulation + membrane enrichment trend)
2	C178 palmitoylation enhanced	C178	S-palmitoylation	ZDHHC4/5/20	Moderate (consistent direction, requires ABE confirmation)
3	S71 inhibitory phosphorylation as compensatory feedback	S71	Phosphoserine	AKT1	Indirect (AKT1 upregulated; S71 = AKT substrate; framed as compensatory negative feedback)

Figure Legends

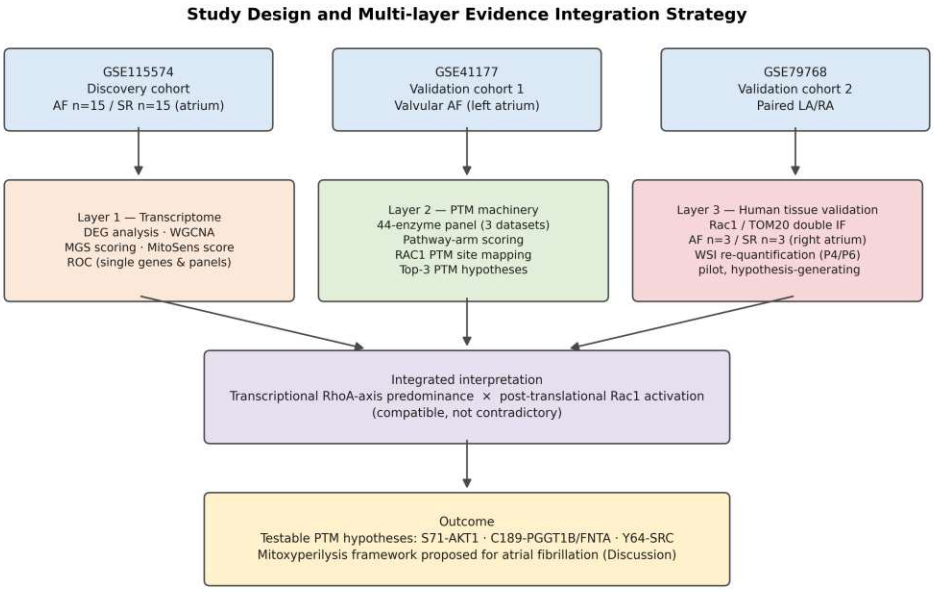


Figure 1. Study design and multi-layer evidence integration strategy. Schematic overview of the study design. Three public transcriptomic datasets (GSE115574 as discovery, GSE41177 and GSE79768 as validation) were analyzed through a three-layer evidence framework: (1) transcriptomic differential expression and pathway scoring, (2) PTM enzyme panel and modification hypothesis generation, and (3) experimental validation via Rac1 immunofluorescence in human right atrial tissue. MGS = Mitoxyperilysis Gene Set; PTM = post-translational modification; IF = immunofluorescence.

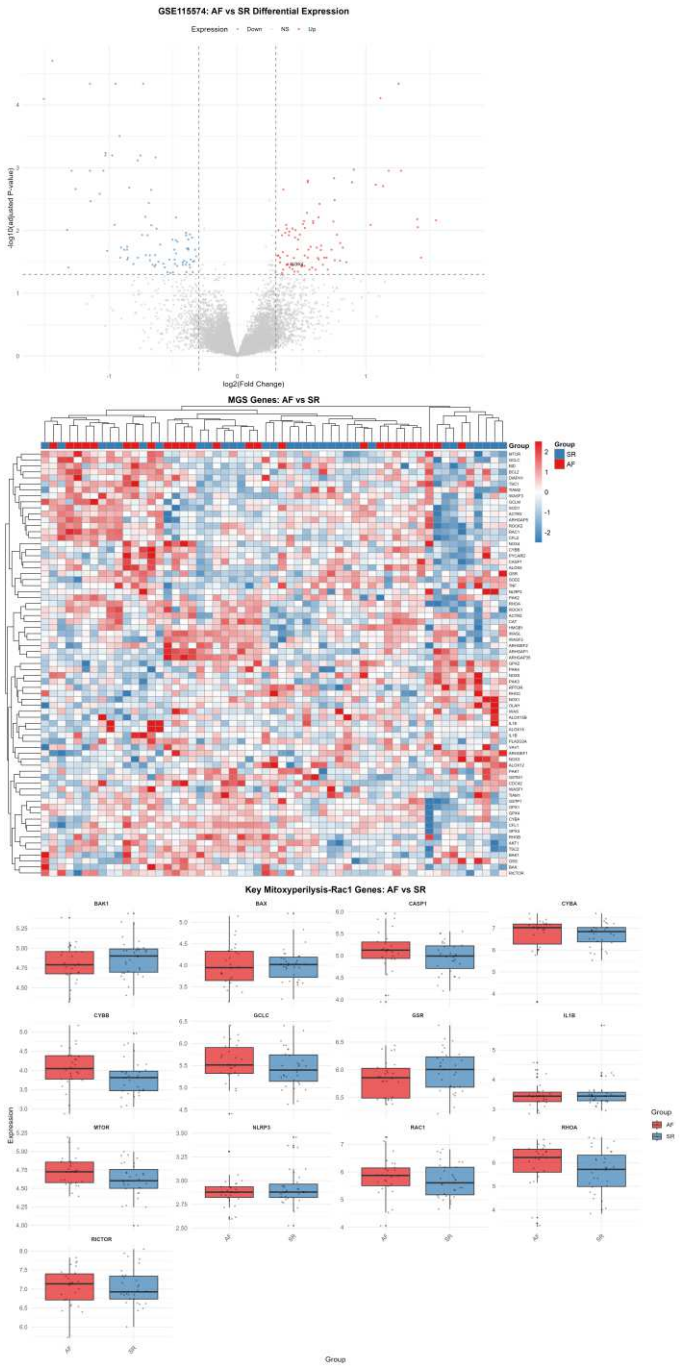


Figure 2. Differential expression and MGS gene patterns in GSE115574. (a) Volcano plot of differentially expressed genes (DEGs) between AF and SR groups in GSE115574 ($|\log_2FC| > 0.2$, adj. $P < 0.05$). 170 DEGs were identified, including 3 MGS genes significantly altered. (b) Heatmap of 77 MGS genes showing expression patterns across

samples. (c) Boxplots of key MGS genes with significant differences. AF = atrial fibrillation; SR = sinus rhythm; MGS = Mitoxyperilysis Gene Set.

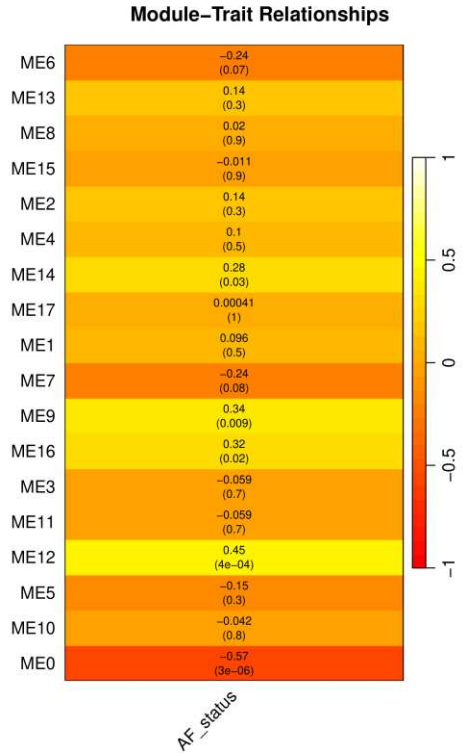


Figure 3. WGCNA module-trait relationships. Module-trait relationship heatmap from WGCNA analysis in GSE115574. Each row represents a module and each column a clinical trait. Correlation coefficients and P values are shown.

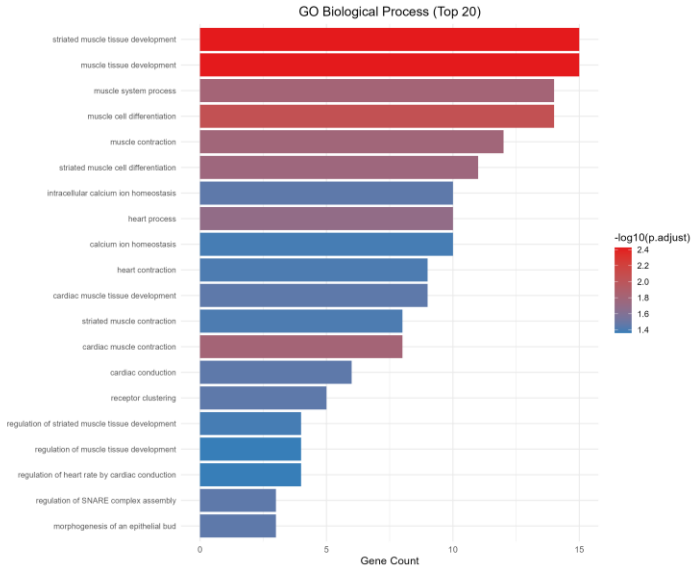


Figure 4. GO biological process enrichment of DEGs in GSE115574. Barplot of the top enriched Gene Ontology (GO) biological process terms among the 170 DEGs (adjusted $P < 0.05$, clusterProfiler).

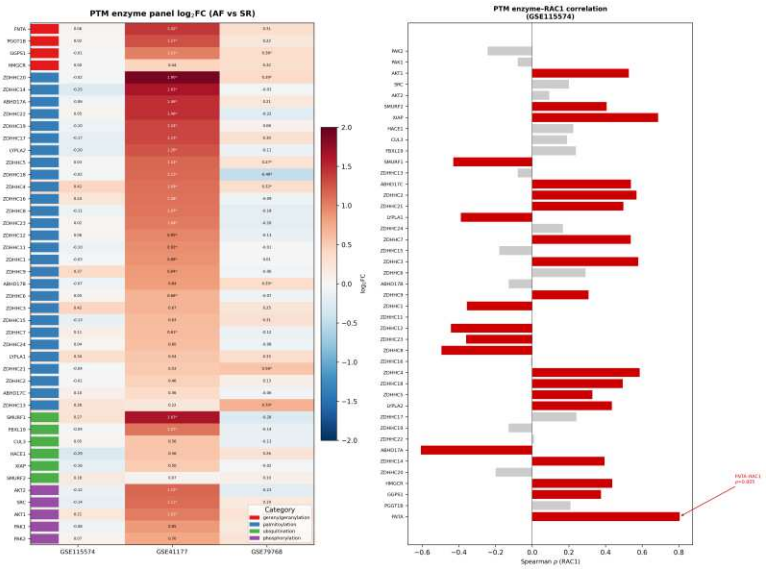


Figure 5. PTM enzyme panel expression and correlation with RAC1/PAK1. (a) Heatmap of 44 PTM enzyme genes showing $\log_2$ fold changes (AF vs SR) across three datasets. Stars indicate statistical significance (adj. $P < 0.05$). Five genes showed cross-

dataset concordant upregulation (GGPS1, ZDHHC4, ZDHHC5, ZDHHC20, AKT1). (b) Spearman correlations between PTM enzymes and RAC1 expression in GSE115574. FNTA–RAC1 $\rho = 0.805$ ($P < 1 \times 10^{-5}$) was the strongest correlation; enzyme–PAK1 correlations are shown in Figure S6.

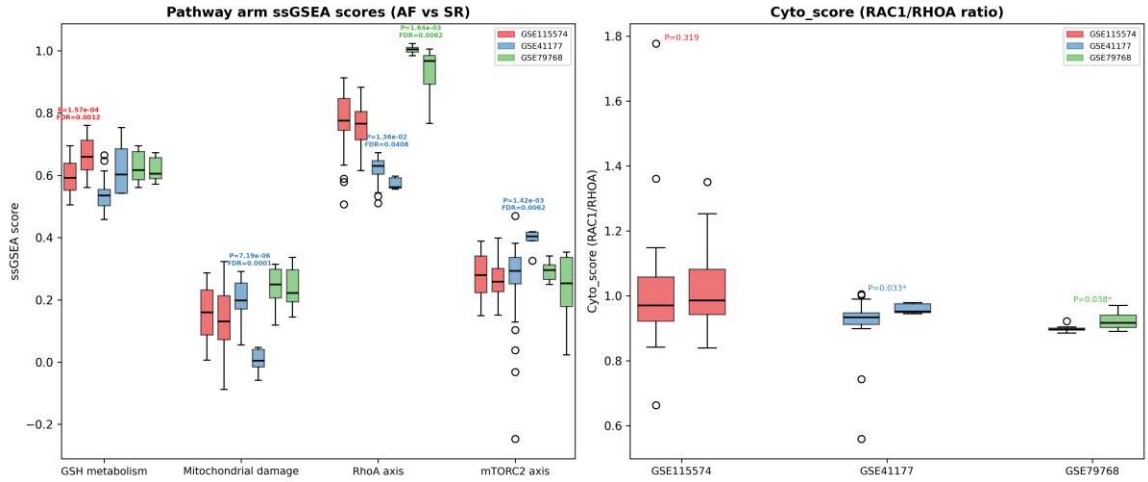
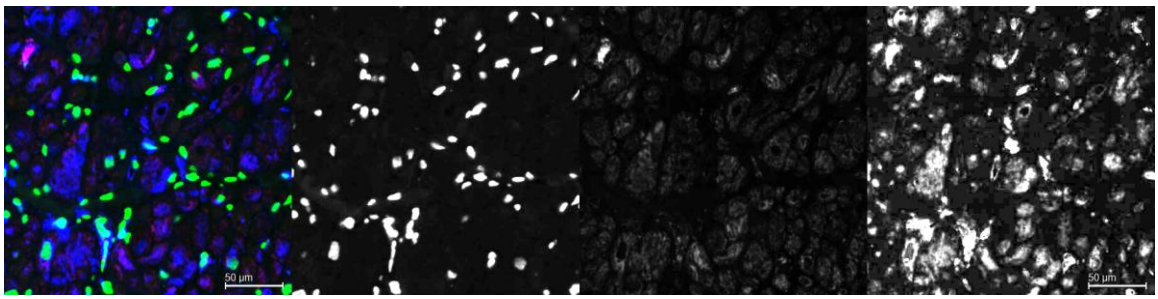
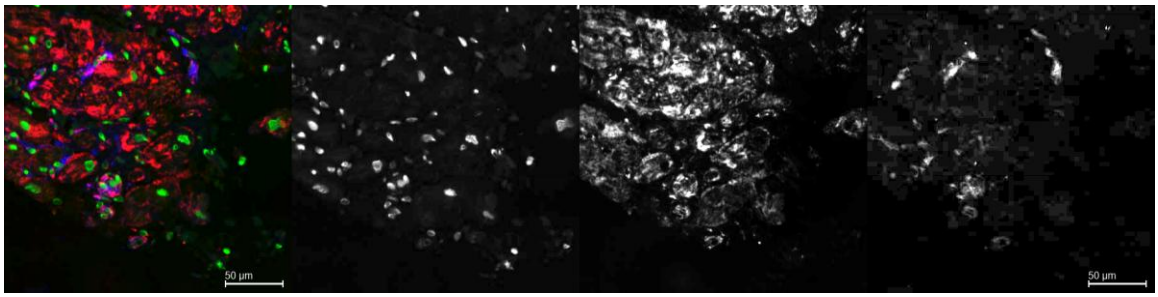
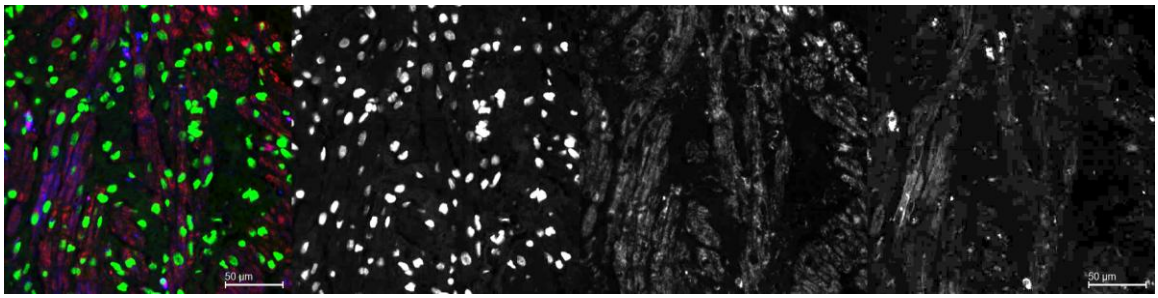
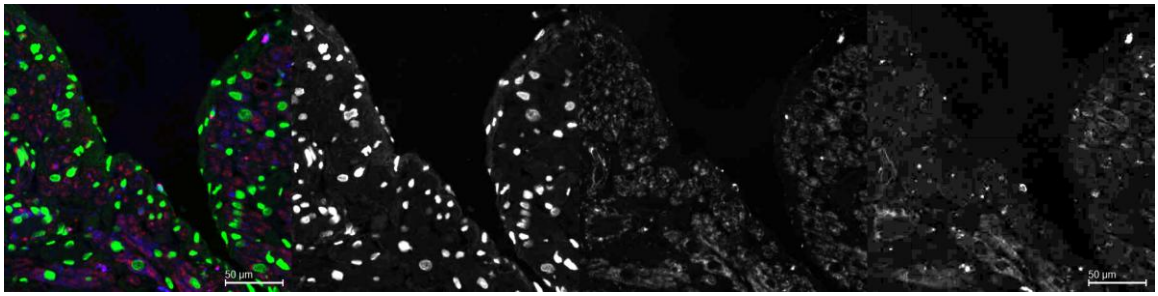


Figure 6. Pathway arm scoring and Rac1/RhoA balance analysis. (a) Boxplots of ssGSEA-derived pathway arm scores across three datasets. GSH metabolism was significantly downregulated in GSE115574 ($P = 1.57 \times 10^{-4}$, FDR = 0.0012). Mitochondrial damage arm was upregulated in GSE41177 ($P = 7.19 \times 10^{-6}$, FDR = 1.08×10^{-4}). RhoA axis showed concordant upregulation in GSE41177 (FDR = 0.041) and GSE79768 (FDR = 0.0062). (b) Cyto_score (RAC1/RHOA transcriptional ratio) was consistently lower in AF across all three datasets (negative finding).




50 µm
50 µm


50 µm
50 µm


50 µm
50 µm

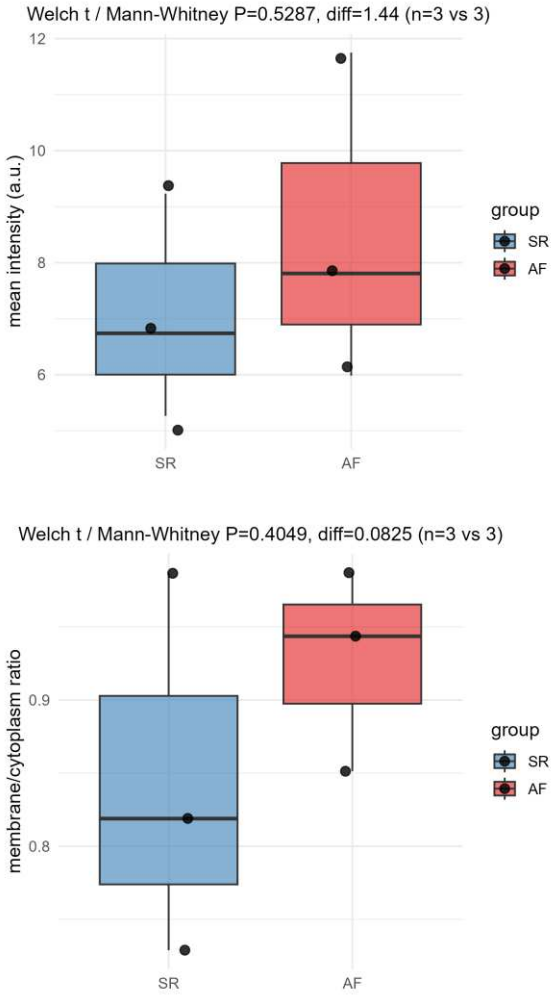


Figure 7. Rac1 immunofluorescence validation in human atrial tissue (pilot). (a) Representative immunofluorescence images of TOM20 (green), Rac1 (red), and DAPI (blue) in human right atrial tissue from AF and SR patients. Representative fields were selected from the quantitative sampling set (seed 20260813) by proximity to group-median values with documented morphology criteria. Scale bar = 50 μm. (b) Rac1 mean intensity per sample (AF: 8.51 ± 2.95 vs SR: 7.08 ± 2.00, P = 0.53, Welch's t-test); direction was consistent under robust estimators (trimmed mean: 7.96 vs 6.67, P = 0.56; median: 6.04 vs 5.92, P = 0.93). (c) Membrane-to-cytoplasm ratio (AF: 0.93 ± 0.07 vs

SR: 0.84 ± 0.13, P = 0.40). n = 3/group, 8 fields/sample, Level 2 quantification. Data are mean ± SD; exact P values reported (pilot validation, underpowered at n = 3/group).

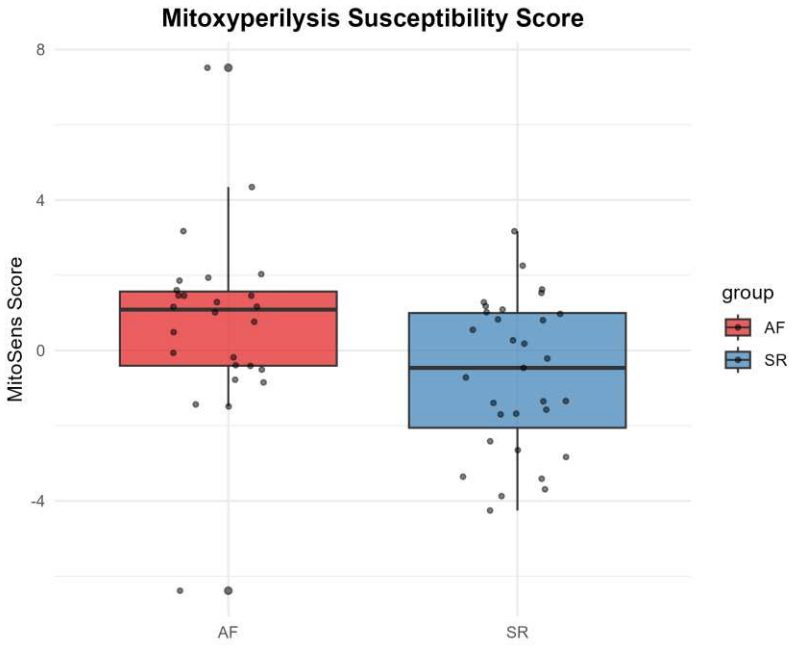


Figure 8. MitoSens score in the discovery cohort GSE115574. Boxplot of the MitoSens composite score in AF versus SR groups (0.776 vs −0.651, P = 0.012). Cross-dataset validation is shown in Figures S1–S4 (GSE41177: AUC = 0.841, P = 0.014; GSE79768: AUC = 0.566, P = 0.656).

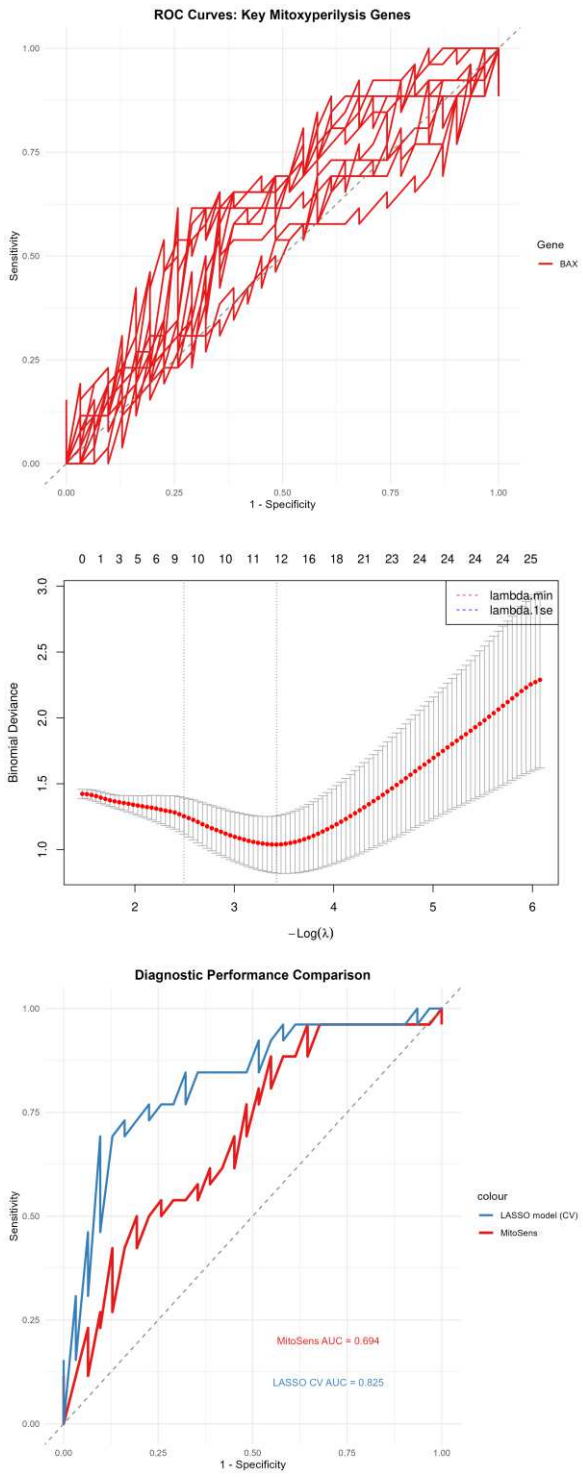


Figure 9. Diagnostic performance evaluation. (a) ROC curves for individual genes in GSE115574. (b) LASSO cross-validation for feature selection. (c) Comparison of ROC performance between MitoSens score and other models.

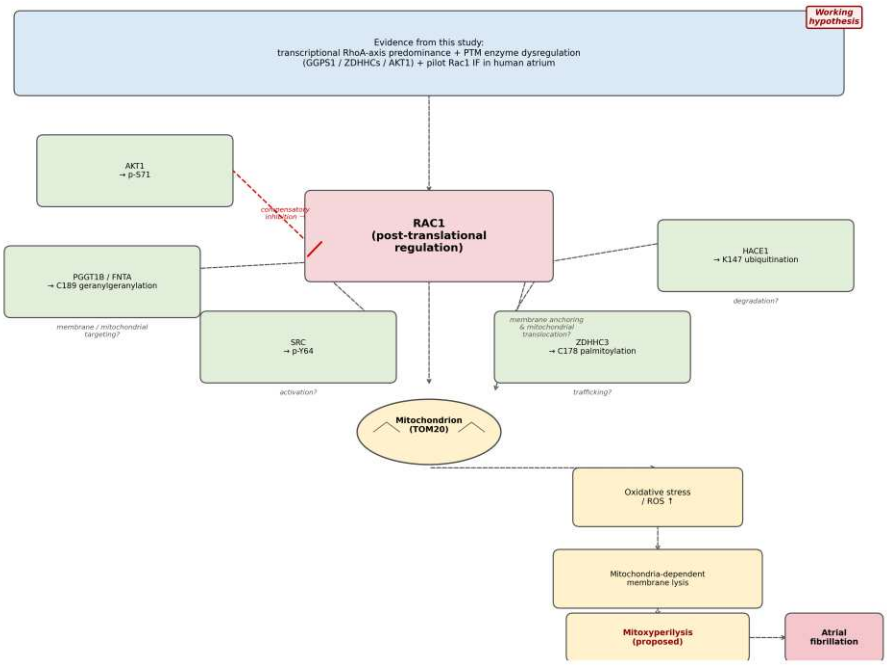


Figure 10. Proposed mechanism: modification-driven Rac1 activation in AF. In AF atrial tissue, RAC1 mRNA expression remains unchanged (transcription-static), while geranylgeranylation (C189) and palmitoylation (C178) machinery is transcriptionally upregulated, promoting Rac1 membrane anchoring and mitochondrial translocation (post-translational activation). The transcriptional RAC1/RHOA ratio (Cyto_score) is paradoxically lower in AF, indicating RhoA relative dominance at the transcript level. Mitoxyperilysis-related pathways (GSH metabolism↓, mitochondrial damage↑) provide a permissive oxidative background. Dashed lines indicate hypothetical connections requiring further validation.

Supplementary Files

This is a list of supplementary files associated with this preprint. Click to download.

- PTMenzymepanel44genescompletegenelistwithcategoryannotations.xlsx
- MitoxyperilysisGeneSet77genescompletegenelistwithliteraturesources.xlsx
- SupplementaryFiguresS1S7.doc